Dark Matter and the Early Formation of Supermassive Black Holes

Andrew Imai, Grant J. Mathews, Guobao Tang, and Brian Zhang¹

¹Center for Astrophysics, Department of Physics and Astronomy, University of Notre Dame, Notre Dame, Indiana, 46556, USA

ABSTRACT

We investigate the growth of supermassive black holes (SMBHs) at high redshift ($z \ge 10$) from a combination of dark matter capture, black-hole mergers, and gas accretion. It has previously been shown that SMBHs can form by $z \approx 10$ via black-hole mergers, Eddington-limited Bondi gas accretion and tidal disruption events with stars within dense nuclear clusters. Here, we show that the capture of collisionless dark matter by a growing SMBH also substantially contributes, in some cases by an order of magnitude to the final SMBH mass. In particular, we show that a small seed stellar-remnant black hole can more easily reach $> 10^7 \ {\rm M}_{\odot}$ by z = 10 in the core of dense nuclear star clusters when dark matter is included. This remains true for either cold dark matter or ultralight dark matter if the mass of the ULDM particle is $\gtrsim 10^{-20}$ eV. We highlight the unique evolution of ULDM capture by the growing SMBH when the ULDM de Broglie wavelength exceeds the initial nuclear star cluster half-mass radius.

Keywords: Supermassive black holes (1663) — Dark matter (353) — Star clusters (1567)

1. INTRODUCTION

A significant problem in modern cosmology is the observation that supermassive black holes (SMBHs) (on the order of $10^6-10^8~{\rm M}_{\odot}$) have formed much earlier than expected by stellar black hole formation and accretion (Greene et al. 2024; Natarajan et al. 2024; Juodžbalis et al. 2024; Maiolino et al. 2024). In particular, the James Webb Space Telescope has detected a $4\times10^7~{\rm M}_{\odot}$ SMBH in an active galactic nucleus as early as $z\approx10$ (Natarajan et al. 2024), suggesting that this SMBH could have formed 200-400 Myr after photon decoupling.

Various attempts have been made to explain the early formation of SMBHs, including the direct collapse of pristine gas clouds (Agarwal et al. 2014; Latif et al. 2022), accretion rates higher than the Eddington limit (super-Eddington accretion) (Davies et al. 2011; Piana et al. 2024; Trinca et al. 2024), and growth from an initial seed black hole on the order of $10~\rm M_{\odot}$ (Begelman et al. 2006; Latif et al. 2022; Greene et al. 2024; Kritos et al. 2024a; Liempi et al. 2025). In the present work, we expand on the latter scenario by exploring the additional contribution from the capture of Cold Dark Matter (CDM) or ultralight dark matter (ULDM). We show that the inclusion of dark-matter accretion relaxes

Email: aimai@nd.edu, gmathews@nd.edu

the conditions required for the early formation of supermassive black holes in dense nuclear star clusters.

1.1. Nuclear Star Clusters

We consider the growth of a central seed black hole within a dense and massive nuclear star cluster (NSC) (Biernacki et al. 2017). Such clusters exist at the center of most galaxies and typically have a mass range of $10^5 - 10^9 \, \mathrm{M}_{\odot}$ (Neumayer et al. 2020). Their effective radii are not larger than 2 to 5 parsecs and can be much smaller. They are a natural environment for the growth of SMBHs (Antonini 2013).

Theoretical studies (Volonteri et al. 2008) have suggested that the central regions of proto-galaxies may undergo fragmentation, giving rise to dense stellar clusters that contain millions of metal-poor stars. These clusters are predicted to have very compact structures, with half-mass radii typically less than 0.5 pc (Devecchi et al. 2010). However, no clusters with radii smaller than ~ 1 parsec have yet been detected (Vanzella et al. 2023).

In this work, we consider a model in which an initial central stellar seed black hole becomes the site for runaway accretion of gas, stars, remnants, and dark matter (DM). This is a variation of the approach by (Kritos et al. 2024b) who only considered the combined effects of the black hole mergers and Eddington-limited gas accretion in NSCs to form SMBHs in their numerical code NUCE (Nuclear Cluster Evolution). Here we

modify NUCE to include the presence and evolution of CDM and ULDM. We find that DM capture can dominate overwhelmingly the contribution to the final SMBH mass, while somewhat relaxing the requirement of a high concentration of gas and stars.

1.2. Initial Conditions

For the present demonstration, we take the initial seed black hole (BH) to be 30 ${\rm M}_{\odot}$. This is a conservative estimate of the mass of an initial BH that would form from the collapse of the Population III stars in the early universe (Xu et al. 2013; Susa et al. 2014). The stars in the model were taken to obey a Kroupa initial mass function (Kroupa 2002) with a mean stellar mass of 0.59 ${\rm M}_{\odot}$.

For simplicity, we consider models that assume a uniform density distribution of DM, stars, and gas within a small volume at the center of the NSC.

1.3. Simulation of DM content in NSCs

The dark matter distribution in NSCs is not known. In principle, the DM abundance could be very high as slow-moving CDM resulting 3-body gravitational interactions migrate to the center. As guidance for this, we have identified a $6.1 \times 10^8 \ \mathrm{M}_{\odot}$ SMBH at z=0 in the TNG50 run of the IllustrisTNG simulation (Nelson et al. 2019; Pillepich et al. 2019). We then analyzed the structure of the pre-SMBH at $z\approx 20$.

The IllustrisTNG simulations are based upon initial conditions in a Λ CDM cosmology with cosmological parameters from the Planck Collaboration (Planck Collaboration et al. 2016), i.e., $\Omega_m=0.3089$ in which $\Omega_{dm}=0.2603$ and $\Omega_b=0.0486$, $\Omega_{\Lambda}=0.6911$, $H_0=100h$ km/s/Mpc with h=0.6774, $\sigma_8=0.8159$ and $n_s=0.9667$. The simulations began at z=127 and evolved to the current epoch at z=0. The TNG50 simulations use periodic boundary conditions in co-moving coordinates with a box size of 35 Mpc/h (51.7 Mpc). The smoothed particle hydrodynamics includes a resolution of 8×10^4 M $_{\odot}$ for baryonic matter and 4.5×10^5 M $_{\odot}$ for DM. This limits the resolution for small volumes with few particles. Nevertheless, the simulation includes the identification of SMBH formation.

In the TNG cosmological simulations, a seed black hole with mass $\rm M_{seed}$ is placed at the center of a halo whenever the friends-of-friends (FoF) halo finder identifies a halo more massive than a threshold mass that does not yet contain a black hole (Weinberger et al. 2017). The potentially sluggish growth of black holes at high redshift is avoided by selecting a large seed mass of $8\times 10^5~h^{-1}~\rm M_{\odot}$. For this case, the seed black hole did not appear until z=6.49 at $t\approx 840$ Myr.

Once BHs are seeded in massive halos of the TNG50 simulation, they then accrete nearby gas at the Eddington-limited Bondi rate (Nelson et al. 2019). In the system examined here, a central BH begins to form during a significant accretion event at z=6.49. However, in this system, the BH mass does not grow to 10^7 M $_{\odot}$ until about 2 Gyr into the simulation. Nevertheless, this is a useful example in which to examine the relative contributions of baryonic and dark matter to the growth of the SMBH.

Figure 1 shows the radial density profiles of dark matter and total baryonic matter at the center of the identified SMBH-forming system at z=20. The innermost radii ($r \lesssim 30-40~\rm pc$) fall below the resolution limit of the simulation. Nevertheless, this figure shows that the DM and baryonic density profiles fit reasonably well with a Navarro-Frenk-White (NFW) profile (Navarro 2001; Klypin et al. 2002):

$$\rho_{\text{NFW}}(r) = \frac{\rho_s}{(r/r_s)(1 + r/r_s)^2},$$
(1)

where r_s is the scale radius, and ρ_s is a characteristic density scale. The best-fitting parameters are found to be $(\rho_s, r_s) = (0.096 \text{ M}_{\odot}\text{pc}^{-3}, 2670.17 \text{ pc})$ for the dark matter density profile and $(\rho_s, r_s) = (0.006 \text{ M}_{\odot} \text{ pc}^{-3}, 3068.11 \text{ pc})$ for the total baryon density profile.

Based upon this, one could conclude that the ratio of DM-to-baryonic matter could be > 10 in the dense central region. However, allowing for a possible core-cusp correction, we conservatively adopt a DM-to-baryonic matter ratio of $\rho_{\rm DM}/\rho_{\rm M} \approx \Omega_{\rm DM}/\Omega_{\rm M} \approx 5$ from the Planck results. However, we also consider models with substantially more DM or no DM within the NSC.

We also examine the effect of ULDM on the growth of the SMBH. ULDM is often modeled as a free scalar field with a very small mass μ_s . In the non-relativistic limit, the configuration of such a field under the influence of gravity is governed by the Schrödinger-Poisson equations. The quasi-stationary, ground-state solutions of these equations are known as solitons, where quantum pressure exactly balances gravitational self-attraction.

Figure 2 shows an example of the soliton profile for an ULDM field mass of 10^{-20} eV and a NSC half-mass radius of 0.5 pc. Fixing the DM-to-baryonic matter ratio to be ≈ 5 , for this example, we calculate the radius of the soliton core to be ≈ 0.34 pc and the central density to be $\approx 1.41 \times 10^9 \ \mathrm{M}_{\odot} \ \mathrm{pc}^{-1}$. Note that the soliton core radius is comparable to the half-mass radius of the NSC. As described below, this causes differences in the SMBH growth when ULDM is included.

In order to obtain an SMBH at the upper end of the $10^6-10^8~{\rm M}_\odot$ range, we adopt models with a total NSC

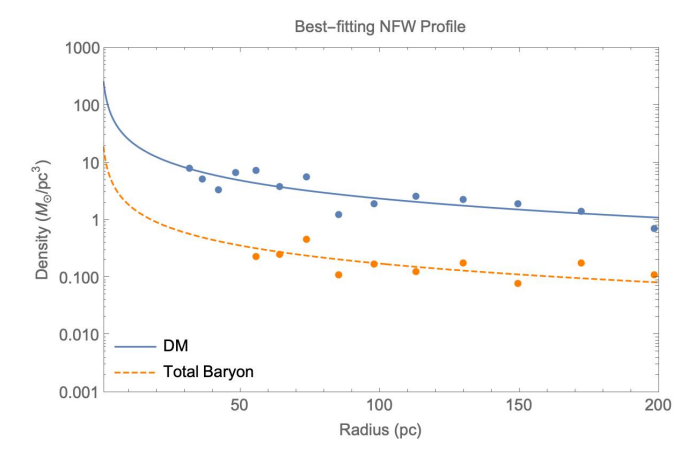


Figure 1. Radial density profiles at redshift $z\approx 20$ of dark matter (blue points) and total baryonic matter (orange points) extracted from the inner 200 pc of a galaxy that contains a $6\times 10^8~{\rm M}_{\odot}$ SMBH at z=0 within TNG50 simulation. The solid (DM) and dashed (baryon) lines represent the best-fitting Navarro–Frenk–White (NFW) profiles to each component.

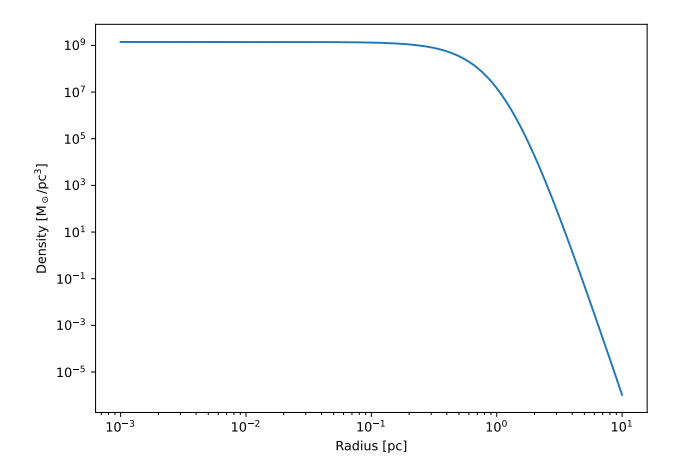


Figure 2. Soliton profile for scalar field of mass $\mu_s = 10^{-20}$ eV associated with a model with a cluster half-mass radius of 0.50 pc.

mass of 8×10^8 M_{\odot} (Turner 1991). For baryonic matter, we took the initial star-to-gas mass ratio to be 4:1. We simulate clusters with initial half-mass radii of varying sizes (0.1, 0.2, 0.5, and 1.0 pc). These initial radii are somewhat larger than those adopted by Kritos et al. (2024b) who considered an initial half-mass radius of 0.1 pc.

The central BH grows through a combination of stellar BH mergers, dark-matter capture, and gas accretion, along with tidal disruption events with stars as described in the next section and in Kritos et al. (2024b). The baryonic gas decreases exponentially over a character-

istic gas expulsion timescale $\tau_{\rm ge}$ and is taken to have a sound speed of 10 km s⁻¹.

2. THE MODEL

The growth of the central black hole in the nuclear star cluster model considered here is described in part by the following set of coupled equations modified from those of Kritos et al. (2024b):

$$\frac{d\overline{m}_*}{dt} = -\nu \frac{\overline{m}_*}{t} \Theta(t - t_{\rm se})$$
 (2a)

$$\frac{dN_*}{dt} = -\xi_e \frac{N_*}{\tau_{\rm rh}} - R_{\rm TDE} \tag{2b}$$

$$\frac{dN_{\rm BH}}{dt} = -k_{\rm ejs}R_{\rm 3bb} \tag{2c}$$

$$\frac{dM_{\rm g}}{dt} = -\frac{M_{\rm g}}{\tau_{\rm ge}} - \dot{M}_{\rm acc} \tag{2d}$$

$$\frac{dM_{\rm BH}}{dt} = \dot{M}_{\rm acc} + f_{\rm TDE}\overline{m}_* R_{\rm TDE}$$
 (2e)

 $+ \rho_{\mathrm{DM}} \langle \sigma_{\mathrm{capt}} v_{\mathrm{DM}} \rangle$

$$\frac{dr_{\rm h}}{dt} = \left(\frac{\zeta r_{\rm h}}{\tau_{\rm rh}} + \frac{2r_{\rm h}}{M_{\rm cl}} \frac{dM_{\rm cl}}{dt}\right) \Theta(t - \tau_{\rm cc}) \qquad (2f)$$

$$- \frac{r_{\rm h}}{M_{\rm cl}} \left(N_* \frac{d\overline{m}_*}{dt} - \frac{M_{\rm g}}{\tau_{\rm ge}}\right)$$

The first equation (2a) describes the rate of change of the average stellar mass \overline{m}_* after a stellar evolution time $t_{\rm se}=2$ Myr (Alexander et al. 2014), where $\Theta(t-t_{\rm se})$ is the Heaviside step function. The loss of massive stars at the end of their life will cause the averaged mass (integrated over the stellar IMF) to shift to smaller values in time. This evolution can be approximated by a power law (Alexander et al. 2014):

$$\overline{m}_* = \overline{m}_0 (t/\tau_{\rm se})^{-\nu},\tag{3}$$

where $\nu = 0.07$.

The first term in the second equation (2b) is an approximate fit to numerical simulations (Alexander et al. 2014) of the loss of the number of stars N_* due to relaxation-driven stellar escape. Here, the half-mass relaxation time of the cluster $\tau_{\rm rh}$ is the characteristic time over which a fraction ψ of the total energy in the cluster is redistributed throughout the cluster via two-body relaxation. This can be approximated as

$$\tau_{\rm rh} = 0.138 \sqrt{\frac{M_{\rm cl} r_{\rm h}^3}{G} \frac{1}{\overline{m}_* \psi \ln \Lambda}} \quad , \tag{4}$$

with

$$\psi = 1 + S_{\rm BH} \tag{5}$$

where $S_{\rm BH}$ is the Spitzer parameter given by

$$S_{\rm BH} = \left(\frac{N_{\rm BH}}{N_{\rm star}}\right) \times \left(\frac{m_{\rm BH}}{m_{\rm star}}\right)^{\frac{5}{2}}.$$
 (6)

The second term in Eq. (2b) is the loss of stars due to tidal disruption events. If one only considers the disruption of stars due to the central black hole, then the TDE rate is

$$R_{\rm TDE} = \dot{E}_{\rm cl}/Q_{\rm TDE}$$
 , (7)

where

$$Q_{\rm TDE} = \frac{GM_{\rm BH}\overline{m}_*}{2r_{\rm T}} \tag{8}$$

is the heat released by each tidal disruption event and $r_{\rm T}$ is the tidal radius.

The evolution of the number of stellar black holes in Eq. (2c) is governed by the ejection of BHs through three-body interactions. The parameter $k_{\rm ejs}$ is the efficiency of BH ejection by 3-body interactions, and $R_{\rm 3bb}$ is the rate of formation of the three-body systems (Antonini & Gieles 2020).

The next equation (2d) accounts for the loss of gas $M_{\rm g}$ from the cluster through a characteristic gas expulsion timescale, $\tau_{\rm ge}=100$ Myr, and accretion onto the central BH computed using an Eddington-limited Bondi accretion rate, $\dot{M}_{\rm acc}$, as described below (Kritos et al. 2024b).

Eq. (2e) gives the adjusted mass accumulation rate of the central seed black hole due to gas accretion, stellar tidal disruption and dark matter capture. The first term is the Eddington-limited Bondi rate, $\dot{M}_{\rm acc}$, for gas accretion as discussed in (Antonini 2013) and (Kritos et al. 2024b), i.e. for hydrogen gas accretion, the maximum Bondi accretion rate is:

$$\dot{M}_{\rm acc} = \frac{4\pi G M_{\rm BH} m_p}{\eta c \sigma_T} \quad , \tag{9}$$

where m_p is the proton mass, $\eta=0.1$ is the radiative efficiency, and σ_T is the Thomson scattering cross section. When gas accretion dominates the growth of the black hole mass, this leads to exponential growth $M_{\rm BH}=M_0\exp{(t/\tau)}$ where

$$\tau = \frac{\eta c \sigma_T}{4\pi G m_p} \approx 50 \text{ Myr} ,$$
 (10)

is the Salpeter timescale.

The second term in Eq. (2e) accounts for tidal disruption events. Here, $f_{\rm TDE}$ is the fraction of the stellar mass in stellar tidal disruption events that accrete onto the central BH. The variable \overline{m}_* is the mean mass of stars, and $R_{\rm TDE}$ is the rate of tidal disruption events. The third term describes the growth of the central BH by DM accretion in the cluster. The average is over the DM velocity distribution as described below.

In addition to the above, the central BH growth rate is incremented at each time step from the BH mergers as described in Kritos et al. (2024b). The number of 3-body BH systems is given by $R_{\rm 3bb}dt$. These are sampled based upon a Poisson distribution and assigned masses and semi-major axes according to the initial hardness parameter of Morscher et al. (2015). The remnant mass, spin and kick velocities are assigned according to the relativistic numerical simulations of Gerosa & Kesden (2016).

A fraction of these systems form a BH binary after merger. The simulation then checks whether the resulting binary has a larger gravitational radius than the ejection radius. If so, then the binary remains within the NSC. If the kick velocity is less than the escape velocity the mass of the central black hole $M_{\rm BH}$ is discretely increased by the mass of the binary remnant. The black hole spin, and number of BHs is also updated. Otherwise, the remnant is ejected.

The last equation, (2f), gives the rate of expansion of the half-mass radius $r_{\rm h}$. It depends on two contributions. The first term is the expansion of the cluster from the half-mass relaxation timescale and mass change. It can be derived by directly differentiating the equation relating the total cluster energy $E_{\rm cl}$, the total cluster mass $M_{\rm cl}$, and the half-mass radius $r_{\rm h}$ in virial equilibrium:

$$E_{\rm cl} = -\kappa \frac{GM_{\rm cl}^2}{2r_{\rm h}} \quad , \tag{11}$$

where $\kappa = 0.4$ for most spherical stellar systems (Spitzer Jr 1969), and using Hénon's principle (Hénon 1961, 1965; Gieles et al. 2011):

$$\frac{\dot{E}_{\rm cl}}{E_{\rm cl}} = -\frac{\zeta}{\tau_{\rm rh}},\tag{12}$$

where $\tau_{\rm rh}$, defined by Eq. (4), is the characteristic timescale over which a fraction $\zeta \simeq 0.1$ of the total cluster energy can be transferred throughout the cluster via two-body relaxation. The quantity $\tau_{\rm cc}$ is the timescale for core collapse, i.e. the timescale for BHs to reach the center and start heating the cluster. This is taken as a fraction of the half-radius relaxation time, i.e. $\tau_{\rm cc} = 0.2\tau_{\rm rh}$ (Portegies Zwart & McMillan 2002).

The second term in Eq. (2f) is derived from the successive disruption and restoration of virial equilibrium following each infinitesimal mass loss event experienced by the cluster, assuming the mass is ejected gradually over a time much longer than the dynamical time $\tau_{\rm rh}$. It is an adiabatic expansion term from gas expulsion (Hills 1980; Kritos et al. 2024b). The expulsion of gas ejected by massive stars and residual gas within the cluster reduces its gravitational binding energy, thereby leading to cluster expansion.

Accretion of CDM onto a centrally growing Schwarzschild black hole of mass $M_{\rm BH}$ can be described by the classical gravitational capture cross section.

$$\sigma_{\rm capt} = \frac{4\pi R_s^2}{(v_{\rm DM}/c)^2}, \quad R_s \equiv \frac{2GM_{\rm BH}}{c^2},$$
 (13)

which applies to any non-relativistic CDM candidate, whether WIMPs, primordial black holes (PBHs), sterile neutrinos, axions, etc. Here, $v_{\rm DM}$ refers to the asymptotic speed of CDM particles far from the black hole.

Note that here we only consider the case of PBHs with a mass much smaller than that of the central accreting BH. For low-mass PBHs ($m_{\rm pbh} \ll M_{\rm BH}$), the formation of a bound binary through gravitational-wave emission (GW capture) is strongly suppressed. The corresponding cross-section is

$$\sigma_{\rm GW} = \frac{kG^2 M^{12/7} \mu^{2/7}}{v_{\rm DM}^{18/7} c^{10/7}} \approx \frac{kR_s^2}{(v_{\rm DM}/c)^{18/7}} \left(\frac{m_{\rm pbh}}{M_{\rm BH}}\right)^{2/7},$$
(14)

with $M \equiv M_{\rm BH} + m_{\rm pbh}$, $\mu \equiv M_{\rm BH} m_{\rm pbh}/(M_{\rm BH} + m_{\rm pbh})$, and $k \equiv (\pi/2)(85\pi/6\sqrt{2})^{2/7}$. $\sigma_{\rm GW}$ is significantly reduced by the small $(m_{\rm pbh}/M_{\rm BH})^{2/7}$ factor. Under any realistic halo velocity dispersion, this factor renders $\sigma_{\rm GW}$ several orders of magnitude smaller than $\sigma_{\rm capt}$. Hence, GW capture of low-mass PBHs can be neglected in the DM accretion process considered here.

We assume that the root mean square (RMS) speed of the CDM is the virial velocity:

$$v_{\rm vir} = \sqrt{\kappa \frac{GM_{\rm cl}}{r_{\rm h}}} \quad . \tag{15}$$

The CDM accretion rate will be dominated by the lowest velocities in the velocity distribution. To account for this, we adopt a Maxwellian distribution for the CDM velocities with an RMS speed given by $v_{\rm vir}$, i.e. the probability of finding DM of velocity $v_{\rm DM}$ within an interval $dv_{\rm DM}$ is:

$$P(v_{\rm DM})dv_{\rm DM} = 4\pi^{-1/2} \frac{v_{\rm DM}^2}{\tilde{v}_{\rm vir}^3} \exp\left(-\frac{v_{\rm DM}^2}{\tilde{v}_{\rm vir}^2}\right) dv_{\rm DM}, (16)$$

where $\tilde{v}_{\rm vir} \equiv \sqrt{\frac{2}{3}} v_{\rm vir}$. Then, the CDM accretion rate can be calculated by

$$\rho_{\rm DM} \langle \sigma_{\rm capt} v_{\rm DM} \rangle = \rho_{\rm DM} \int_0^\infty dv_{\rm DM} \sigma_{\rm capt} v_{\rm DM} P(v_{\rm DM})$$
$$= 8\sqrt{\pi} \rho_{\rm DM} R_s^2 c^2 \tilde{v}_{\rm vir}^{-1} \quad , \tag{17}$$

where $\rho_{\rm DM}$ is the mass density of DM.

The total mass of CDM in the NSC will decrease as particles are captured by the central black hole. The mass of CDM evolves in time according to:

$$\frac{dM_{\rm DM}}{dt} = -\rho_{\rm DM} \langle \sigma_{\rm capt} v_{\rm DM} \rangle. \tag{18}$$

In the case of ULDM, we take the evolution in BH mass due to the accretion of ULDM to be

$$\frac{dM_{\rm BH,ULDM}}{dt} = -\frac{dM_{\rm ULDM}}{dt} = (0.04)R_{\rm s}^2 G^3 M_{\rm sol}^4 \mu_s^6$$
 (19)

as derived in Bucciotti & Trincherini (2023). Here, μ_s is the mass of the scalar field, and we set $\hbar = c = 1$. The density dependence is encoded in $M_{\rm sol}$, which represents the total mass of ULDM that forms solitons enclosed within a radius r (based on the evolving soliton core radius) and is given by

$$M_{\rm sol} = \int_0^r 4\pi r'^2 \,\rho_{\rm sol} \,\mathrm{d}r'.$$
 (20)

Following the derivation in Marsh & Pop (2015), the soliton mass and central density scale with the ULDM de Broglie wavelength as:

$$M_{\rm sol} \propto \lambda^{-1},$$
 (21)

$$\rho_{\rm sol} \propto \lambda^{-4}.$$
(22)

Thus.

$$\rho_{\rm sol} \propto M_{\rm sol}^4.$$
(23)

This scaling is a consequence of the Schrödinger–Poisson equations governing ULDM soliton cores. We adopt this relation to evolve the soliton density in time as:

$$\rho_{\rm sol}(t) = \rho_{\rm sol,0} \left(\frac{M_{\rm sol}(t)}{M_{\rm sol,0}} \right)^4.$$
(24)

3. RESULTS

3.1. Models with CDM

To assess the role of DM in SMBH growth, we considered a variety of scenarios that incorporated DM accretion into the nuclear star cluster model. We show that this modification significantly enhances the growth of a seed BH into an SMBH.

As a first illustration, consider a model with a seed black hole of 30 M_{\odot} embedded in an NSC of initial mass $8\times10^8~M_{\odot}$. We consider uniform CDM and baryonic matter density profiles within an initial cluster virial half-mass radius of 0.10, 0.20, 0.50, and 1 pc. Note that we consider models with larger initial radii than the 0.1 pc half-radius adopted in Kritos et al. (2024b).

The total cluster mass for this example was divided among DM, stars, and gas based upon a DM-to-baryon density ratio of 5, and placing 20% of the baryonic mass in gas. The initial mass in stars is then 80% of the baryonic mass based upon the IMF.

The top panel of Figure 3 shows the evolution of the mass of the SMBH for various initial half-radii and models with and without CDM. All of these models exhibit

an initial gradual growth of the central BH due to the combination of Eddington-limited Bondi accretion and a small amount of DM capture until the core collapse time $\tau_{\rm cc}$.

The growth of the half-mass radius r_h is shown in the second panel of Figure 3. The cluster half-mass radius expands after $t=\tau_{\rm cc}$ according to Eq. (1f). As noted in Kritos et al. (2024b), at $\tau_{\rm cc}$ the system is considered to be virialized and the seed black hole mass can rapidly grow by BH mergers as evidenced in the third and fourth panels of 3. Concurently in our model, the rapid BH growth accelerates the capture of CDM after $\tau_{\rm cc}$ due to the dependence of the capture cross section on the BH mass. This is illustrated by the evolution of $\dot{M}_{\rm DM}$ as shown in the bottom panel of 3.

From Eq. (13), the rate of mass of DM falling into the seed BH scales with the cross section, which in turn scales with the mass of the central black hole.

$$\sigma_{\rm capt} \propto M_{\rm BH}^2$$
 . (25)

Hence, once the seed BH becomes sufficiently large, DM absorption proceeds rapidly. This leads to significant additional SMBH growth until the DM is depleted as shown in the bottom panel of 3.

Figure 3 shows that the most dense cluster with an initial virial half-mass radius of 0.10 parsecs attains an SMBH of $\sim 3 \times 10^7~\rm M_{\odot}$ within 200 Myr, nearly accounting for the observation (Natarajan et al. 2024) of an SMBH of $4 \times 10^7~\rm M_{\odot}$ at z=10 and easily explaining the presence of an SMBH of mass $1.5 \times 10^7~\rm M_{\odot}$ in a near-pristine galaxy at z=7.04 as described by Maiolino et al. (2025). In contrast, the simulation without CDM only produces an SMBH of $\leq 10^7~\rm M_{\odot}$. Hence, the presence of CDM enhances the early growth of the mass of the SMBH by a factor of ~ 3 , thereby providing the dominant contribution to the final mass of the SMBH.

The lower density cluster with a 0.2 pc initial half-mass radius reaches $\sim 2\times 10^7~\rm M_{\odot}$ within approximately 100 Myr. In this case, the simulations without DM only lead to a BH mass of $\sim 4\times 10^6~\rm M_{\odot}$. Hence, in this case the presence of DM enhances the mass of the SMBH by a factor of ~ 5 . The NSC with an $r_h=0.5$ pc reaches $\sim 10^7~\rm M_{\odot}$ within approximately 1000 Myr. In this case, the simulations without DM do not produce an SMBH $> 8\times 10^5~\rm M_{\odot}$ within $10^4~\rm Myr$. Hence, the DM in this case increases the SMBH mass by an order of magnitude.

The case with an initial half-mass radius of 1 pc exhibits a somewhat different evolution. The accretion of gas and DM is depleted after about 400 Myr. However, $\tau_{\rm cc}$ is not achieved until $t\sim 1000$ Myr. Hence, for this model the onset of BH mergers and additional DM cap-

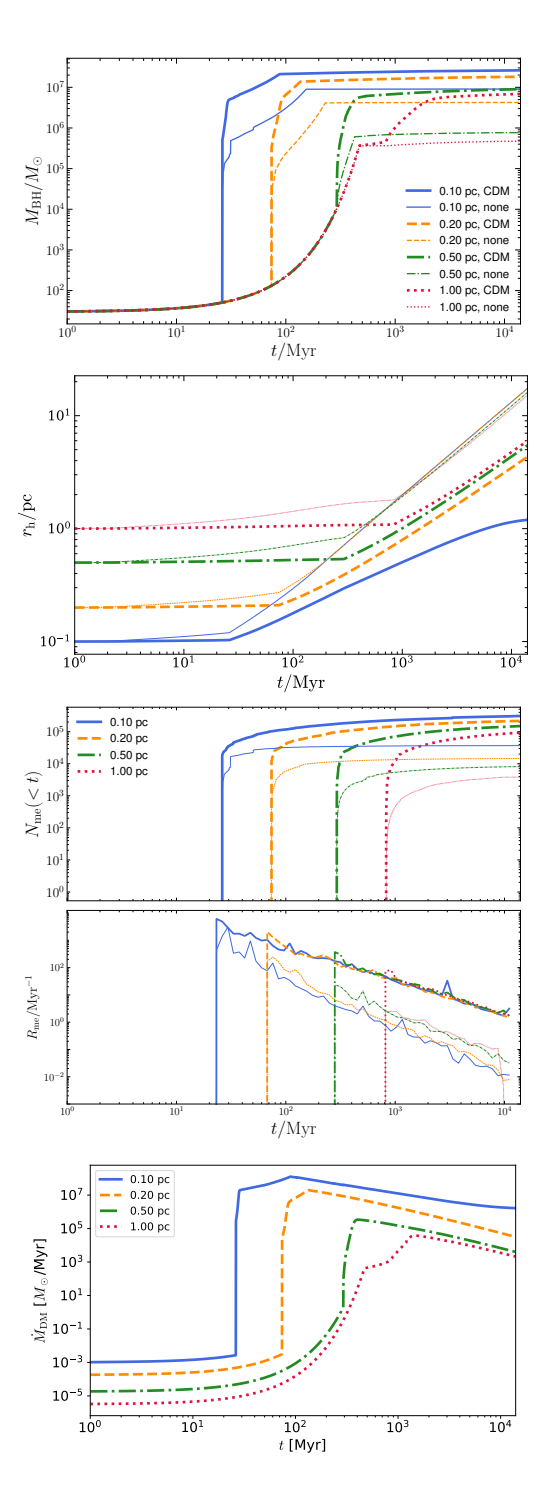


Figure 3. Top panel shows the evolution of the mass of the central black hole beginning with a 30 ${\rm M}_{\odot}$ seed black hole within a cluster of mass of $8\times 10^8~{\rm M}_{\odot}$. Lines correspond to various initial half-mass radii as labeled. Lines are drawn with (CDM) and without (none) the presence of dark matter. The second panel shows the growth of the half-mass radius of the NSC. The NSC begins to grow after the collapse time $\tau_{\rm cc}$ up to the observed sizes of $\sim 1-10~{\rm pc}$. The third panel shows the burst of number of black hole mergers $N_{\rm me}$ once the collapse time has been exceeded. The fourth panel is the corresponding rate $R_{\rm me}$ of BH mergers. The bottom panel shows the rate of dark matter accretion $\dot{M}_{\rm DM}$.

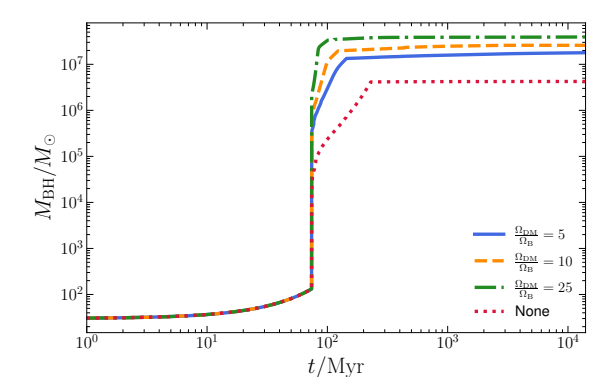


Figure 4. SMBH growth in models with varying DM–to-baryon ratios while maintaining a constant baryon cluster mass. Other parameters are the same as in Figure 3 for the model with an initial half-mass radius of 0.20 pc.

ture appears as a second growth beginning at 1000 Myr after a plateau in BH mass forms at 400 Myr.

In Figure 4 we examine the dependence of SMBH growth on the DM-to-baryon ratio. It has been shown that supermassive black hole growth can increase the DM density at the center of galaxies, creating a spike (Gondolo & Silk 1999; Ferrer et al. 2017; Feng et al. 2025). This could provide the conditions for much higher ratios of DM/Baryons.

Figure 4 shows that higher DM/Baryonic ratios accelerate the formation of the SMBH and lead to a higher SMBH mass. The final SMBH mass is roughly proportional to the DM/Baryon ratio, i.e increasing the ratio from 5 to 10 increases the SMBH mass from 1.8×10^7 to 2.6×10^7 , while increasing the ratio by a factor of 5 increases the SMBH mass from 1.8×10^7 to 4×10^7 .

3.2. Models with ULDM

Figures 5, 6, 7 and 8 illustrate the evolution of SMBH growth in the case of ULDM. Figure 5 shows the growth of the central black hole for the case of the most massive scalar field considered here, $\mu_s=10^{-20}$ eV. This figure shows that ULDM can have an even more dramatic increase in the SMBH mass. For $\mu_s=10^{-20}$ eV, the growth of the central BH occurs in 2 stages. First, there is a rapid SMBH growth rate due to BH mergers once $t>\tau_{\rm cc}$. This shown in Figures 5, and 7 and 8. This occurs for all models with or without ULDM.

For the $\mu_s = 10^{-20}$ eV model, however, there is also a second burst of SMBH growth occurring at $t \geq 1$ Gyr. We attribute this to the following: The gas and stellar BH accretion essentially stops at 200-300 Myr. This can be seen in the no-DM curve and also the cases of lighter ULDM mass as shown in Figure 7. This is due

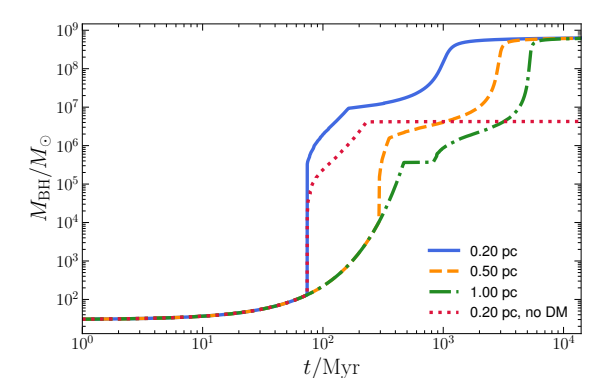


Figure 5. SMBH growth for models with an ULDM mass of $\mu_s = 10^{-20}$ eV scalar field with varying initial half-mass radii. The initial conditions are the same as in Figure 3.

to the expansion of the cluster and diminishing rate of BH mergers.

However, the accretion of ULDM continues because the density of the soliton is constant even though the core radius is expanding. The soliton density remains constant due to its large de Broglie wavelength as shown in Figure 2 and the middle panel of Figure 8. Hence, the ULDM accretion remains robust until the core radius exceeds the soliton radius ~ 1 pc after about 1 Gyr, after which ρ_{sol} decreases rapidly, leading to a decrease in $dM_{\rm BH}/dt$, and the SMBH stops growing as shown in the top and bottom panels of Figure 8.

This highlights a difference in the physics of BH accretion for ULDM. Since the ULDM de Broglie wavelength of the ultralight particle can be comparable to the size of the core radius, e.g. Fig 2, the density remains constant as the core radius grows.

The SMBH growth rate due to ULDM, however, depends sensitively on the scalar field mass, i.e. $\propto \mu_s^6$ as in Eq. (19). Figure 7 shows the growth of the central black hole for various masses of the ultralight scalar particle and an initial core radius of 0.2 pc. For the case of smaller scalar field masses, the second burst of BH growth is suppressed by the μ^6 factor in Eq. (20). This is true even though the Soliton core is much larger for the lighter ULDM masses. Hence, for lighter ULDM masses only the initial burst of BH mergers contributes to the growth of the SMBH.

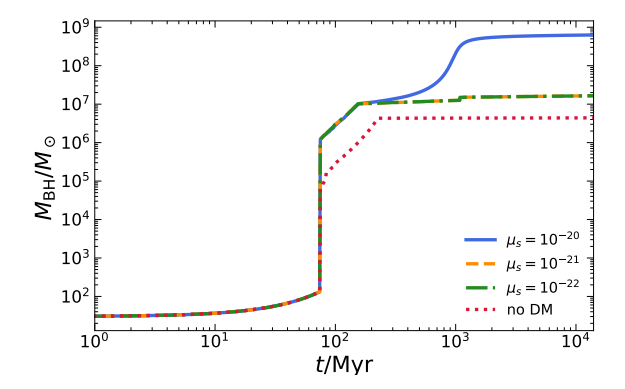


Figure 7. Models with various masses μ_s for the scalar field ultralight DM. The initial conditions are the same as in Figure 3 with an initial half-mass radius of 0.2 pc.

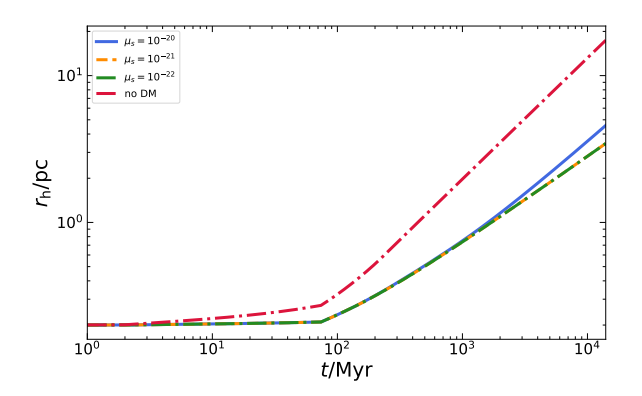


Figure 6. Growth of the half-mass radius of the NSC with various values for the ULDM mass and $r_h = 0.2$ pc.

4. CONCLUSIONS

In summary, we have studied the role of DM in the early growth of a seed stellar black hole into an SMBH in a dense nuclear cluster. We find that with the inclusion of CDM (or ULDM with mass $\mu_s \sim 10^{-20}$ eV), a central seed black hole can more easily grow to the $4\times 10^7~\rm M_{\odot}$ SMBH detected at z=10 by JWST (Natarajan et al. 2024) and easily grows to $1.5\times 10^7~\rm M_{\odot}$ SMBH by z=7.04 as described by Maiolino et al. (2025).

Indeed, depending upon the ratio of DM to baryonic matter, the dark matter can enhance the mass of the SMBH by an order of magnitude or more. We also highlight here the possible unique contribution of ULDM capture at late times due to its large de Broglie wavelength which keeps the soliton density large until the NSC radius expands beyond the size of the de Broglie wavelength of the ULDM.

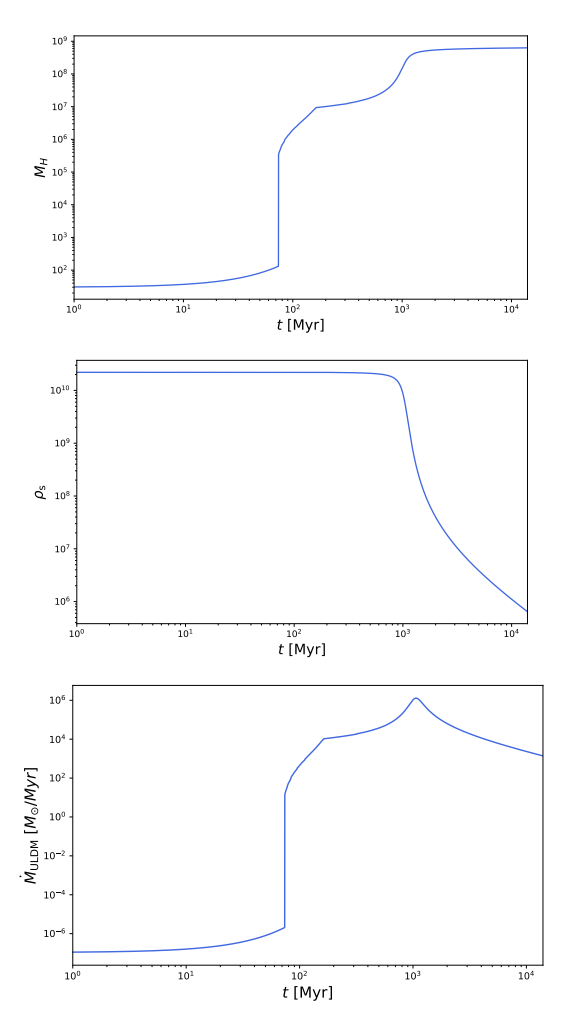


Figure 8. Evolution of SMBH mass (top panel), ULDM density (middle panel) and rate of SMBH growth (bottom panel) for a model with 10^{-20} eV ULDM mass and an initial core radius of 0.2 pc.

ACKNOWLEDGEMENTS

Work at the University of Notre Dame is supported by the U.S. Department of Energy under Nuclear Theory Grant DE-FG02-95-ER40934. We acknowledge support from the University of Notre Dame Center for Research Computing. A. I. thanks Lauren Weiss for helpful discussions on simulation development related to this work.

REFERENCES

Agarwal, B., Dalla Vecchia, C., Johnson, J. L., Khochfar, S., & Paardekooper, J.-P. 2014, Monthly Notices of the Royal Astronomical Society, 443, 648–657,

doi: 10.1093/mnras/stu1112

Alexander, P. E. R., Gieles, M., Lamers, H. J. G. L. M., & Baumgardt, H. 2014, Monthly Notices of the Royal Astronomical Society, 442, 1265–1285,

doi: 10.1093/mnras/stu899

- Antonini, F. 2013, ApJ, 763, 62, doi: 10.1088/0004-637X/763/1/62
- Antonini, F., & Gieles, M. 2020, Monthly Notices of the Royal Astronomical Society, 492, 2936–2954, doi: 10.1093/mnras/stz3584
- Begelman, M. C., Volonteri, M., & Rees, M. J. 2006, MNRAS, 370, 289, doi: 10.1111/j.1365-2966.2006.10467.x
- Biernacki, P., Teyssier, R., & Bleuler, A. 2017, Monthly Notices of the Royal Astronomical Society, 469, 295–313, doi: 10.1093/mnras/stx845
- Bucciotti, B., & Trincherini, E. 2023, Journal of High Energy Physics, 2023, 193, doi: 10.1007/JHEP11(2023)193
- Davies, M. B., Coleman Miller, M., & Bellovary, J. M. 2011, The Astrophysical Journal, 740, L42, doi: 10.1088/2041-8205/740/2/142
- Devecchi, B., Volonteri, M., Colpi, M., & Haardt, F. 2010,
 Mon. Not. Roy. Astron. Soc., 409, 1057,
 doi: 10.1111/j.1365-2966.2010.17363.x
- Feng, C., Tang, Y., & Wu, Y.-L. 2025, arXiv e-prints, arXiv:2506.02937, doi: 10.48550/arXiv.2506.02937
- Ferrer, F., Medeiros da Rosa, A., & Will, C. M. 2017, Phys. Rev. D, 96, 083014, doi: 10.1103/PhysRevD.96.083014
- Gerosa, D., & Kesden, M. 2016, PhRvD, 93, 124066, doi: 10.1103/PhysRevD.93.124066
- Gieles, M., Heggie, D. C., & Zhao, H. 2011, MNRAS, 413, 2509, doi: 10.1111/j.1365-2966.2011.18320.x
- Gondolo, P., & Silk, J. 1999, Phys. Rev. Lett., 83, 1719, doi: 10.1103/PhysRevLett.83.1719
- Greene, J. E., Labbe, I., Goulding, A. D., et al. 2024, ApJ, 964, 39, doi: 10.3847/1538-4357/ad1e5f
- Hénon, M. 1961, Annales d'Astrophysique, Vol. 24, p. 369, 24, 369
- —. 1965, Annales d'Astrophysique, Vol. 28, p. 62, 28, 62
- Hills, J. G. 1980, ApJ, 235, 986, doi: 10.1086/157703
- Juodžbalis, I., Maiolino, R., Baker, W. M., et al. 2024, Nature, 636, 594–597, doi: 10.1038/s41586-024-08210-5
- Klypin, A., Zhao, H., & Somerville, R. S. 2002, ApJ, 573, 597, doi: 10.1086/340656
- Kritos, K., Beckmann, R. S., Silk, J., et al. 2024a, arXiv e-prints, arXiv:2412.15334, doi: 10.48550/arXiv.2412.15334
- Kritos, K., Berti, E., & Silk, J. 2024b, MNRAS, 531, 133, doi: 10.1093/mnras/stae1145
- Kroupa, P. 2002, Science, 295, 82, doi: 10.1126/science.1067524
- Latif, M. A., Whalen, D. J., Khochfar, S., Herrington,
 N. P., & Woods, T. E. 2022, Nature, 607, 48–51,
 doi: 10.1038/s41586-022-04813-y

- Liempi, M., Schleicher, D. R. G., Benson, A., Escala, A., & Vergara, M. C. 2025, A&A, 694, A42, doi: 10.1051/0004-6361/202451672
- Maiolino, R., Scholtz, J., Curtis-Lake, E., et al. 2024, Astronomy & Astrophysics, 691, A145, doi: 10.1051/0004-6361/202347640
- Maiolino, R., Uebler, H., D'Eugenio, F., et al. 2025, arXiv e-prints, arXiv:2505.22567.
 - https://arxiv.org/abs/2505.22567
- Marsh, D. J. E., & Pop, A.-R. 2015, MNRAS, 451, 2479, doi: 10.1093/mnras/stv1050
- Morscher, M., Pattabiraman, B., Rodriguez, C., Rasio,
 F. A., & Umbreit, S. 2015, ApJ, 800, 9,
 doi: 10.1088/0004-637X/800/1/9
- Natarajan, P., Pacucci, F., Ricarte, A., et al. 2024, ApJL, 960, L1, doi: 10.3847/2041-8213/ad0e76
- Navarro, J. F. 2001, arXiv e-prints, astro, doi: 10.48550/arXiv.astro-ph/0110680
- Nelson, D., Pillepich, A., Springel, V., et al. 2019, Monthly Notices of the Royal Astronomical Society, 490, 3234–3261, doi: 10.1093/mnras/stz2306
- Neumayer, N., Seth, A., & Böker, T. 2020, A&A Rv, 28, 4, doi: 10.1007/s00159-020-00125-0
- Piana, O., Pu, H.-Y., & Wu, K. 2024, Monthly Notices of the Royal Astronomical Society, 530, 1732, doi: 10.1093/mnras/stae851
- Pillepich, A., Nelson, D., Springel, V., et al. 2019, MNRAS, 490, 3196, doi: 10.1093/mnras/stz2338
- Planck Collaboration, Ade, P. A. R., Aghanim, N., et al. 2016, A&A, 594, A13, doi: 10.1051/0004-6361/201525830
- Portegies Zwart, S. F., & McMillan, S. L. W. 2002, ApJ, 576, 899, doi: 10.1086/341798
- Spitzer Jr, L. 1969, Astrophysical Journal, vol. 158, p. L139, 158, L139
- Susa, H., Hasegawa, K., & Tominaga, N. 2014, The Astrophysical Journal, 792, 32, doi: 10.1088/0004-637x/792/1/32
- Trinca, A., Valiante, R., Schneider, R., et al. 2024, arXiv e-prints, arXiv:2412.14248, doi: 10.48550/arXiv.2412.14248
- Turner, M. S. 1991, Physica Scripta, 1991, 167, doi: 10.1088/0031-8949/1991/T36/018
- Vanzella, E., Claeyssens, A., Welch, B., et al. 2023, The Astrophysical Journal, 945, 53, doi: 10.3847/1538-4357/acb59a
- Volonteri, M., Lodato, G., & Natarajan, P. 2008, Monthly Notices of the Royal Astronomical Society, 383, 1079, doi: 10.1111/j.1365-2966.2007.12589.x
- Weinberger, R., Springel, V., Hernquist, L., et al. 2017, MNRAS, 465, 3291, doi: 10.1093/mnras/stw2944

Xu, H., Wise, J. H., & Norman, M. L. 2013, The Astrophysical Journal, 773, 83,

doi: 10.1088/0004-637X/773/2/83